EXTENDED PDF FORMAT SPONSORED BY
Tools for Your
Biological Target
sigma.com/biotarget2

Signatures of Majorana Fermions in Hybrid Superconductor-Semiconductor Nanowire Devices

V. Mourik *et al.*

Science **336**, 1003 (2012);
DOI: 10.1126/science.1222360

This copy is for your personal, non-commercial use only.

If you wish to distribute this article to others, you can order high-quality copies for your colleagues, clients, or customers by clicking here.

Permission to republish or repurpose articles or portions of articles can be obtained by following the guidelines here.

The following resources related to this article are available online at www.sciencemag.org (this information is current as of May 29, 2012):

Updated information and services, including high-resolution figures, can be found in the online version of this article at:
http://www.sciencemag.org/content/336/6084/1003.full.html

Supporting Online Material can be found at:
http://www.sciencemag.org/content/suppl/2012/04/11/science.1222360.DC1.html

A list of selected additional articles on the Science Web sites **related to this article** can be found at:
http://www.sciencemag.org/content/336/6084/1003.full.html#related

This article has been **cited by** 1 articles hosted by HighWire Press; see:
http://www.sciencemag.org/content/336/6084/1003.full.html#related-urls

This article appears in the following **subject collections:**
Physics
http://www.sciencemag.org/cgi/collection/physics

Downloaded from www.sciencemag.org on May 29, 2012

Science (print ISSN 0036-8075; online ISSN 1095-9203) is published weekly, except the last week in December, by the American Association for the Advancement of Science, 1200 New York Avenue NW, Washington, DC 20005. Copyright 2012 by the American Association for the Advancement of Science; all rights reserved. The title *Science* is a registered trademark of AAAS.

rather than by microtubule reorganization. Thus, polarization of the DV axis is independent of the formation of the microtubule array that defines the AP axis, as previously proposed.

References and Notes

1. I. Dupin, S. Etienne-Manneville, *Int. J. Biochem. Cell Biol.* **43**, 1698 (2011).
2. A. González-Reyes, H. Elliott, D. St Johnston, *Nature* **375**, 654 (1995).
3. S. Roth, F. S. Neuman-Silberberg, G. Barcelo, T. Schüpbach, *Cell* **81**, 967 (1995).
4. R. Bastock, D. St Johnston, *Curr. Biol.* **18**, R1082 (2008).
5. A. Swan, B. Suter, *Development* **122**, 3577 (1996).
6. A. Swan, T. Nguyen, B. Suter, *Nat. Cell Biol.* **1**, 444 (1999).
7. Y. Lei, R. Warrior, *Dev. Biol.* **226**, 57 (2000).
8. J. E. Duncan, R. Warrior, *Curr. Biol.* **12**, 1982 (2002).
9. J. Januschke *et al.*, *Curr. Biol.* **12**, 1971 (2002).
10. A. Mogilner, G. Oster, *Curr. Biol.* **13**, R721 (2003).
11. E. A. Koch, R. H. Spitzer, *Cell Tissue Res.* **228**, 21 (1983).
12. Y. C. Lee, J. Wolff, *J. Biol. Chem.* **257**, 6306 (1982).
13. J. R. Kardon, R. D. Vale, *Nat. Rev. Mol. Cell Biol.* **10**, 854 (2009).
14. A. E. Radulescu, D. W. Cleveland, *Trends Cell Biol.* **20**, 214 (2010).
15. Y. Mimori-Kiyosue, N. Shiina, S. Tsukita, *Curr. Biol.* **10**, 865 (2000).
16. A. P. Mahowald, J. M. Strassheim, *J. Cell Biol.* **45**, 306 (1970).
17. N. C. Grieder, M. de Cuevas, A. C. Spradling, *Development* **127**, 4253 (2000).
18. J. Bolívar *et al.*, *Development* **128**, 1889 (2001).
19. J. R. Huynh, J. M. Shulman, R. Benton, D. St Johnston, *Development* **128**, 1201 (2001).
20. P. Fichelson, M. Jagut, S. Lepanse, J. A. Lepesant, J. R. Huynh, *Development* **137**, 815 (2010).
21. N. M. Rusan, G. C. Rogers, *Traffic* **10**, 472 (2009).
22. N. R. Stevens, A. A. Raposo, R. Basto, D. St Johnston, J. W. Raff, *Curr. Biol.* **17**, 1498 (2007).
23. J. M. Shulman, R. Benton, D. St Johnston, *Cell* **101**, 377 (2000).
24. P. T. Tran, L. Marsh, V. Doye, S. Inoué, F. Chang, *J. Cell Biol.* **153**, 397 (2001).
25. A. R. Bausch, W. Möller, E. Sackmann, *Biophys. J.* **76**, 573 (1999).
26. R. M. Hochmuth, *J. Biomech.* **33**, 15 (2000).
27. K. Dahlgaard, A. A. Raposo, T. Niccoli, D. St Johnston, *Dev. Cell* **13**, 539 (2007).
28. N. Watanabe, *Proc. Jpn. Acad. Ser. B* **86**, 62 (2010).
29. M. Dogterom, J. W. Kerssemakers, G. Romet-Lemonne, M. E. Janson, *Curr. Opin. Cell Biol.* **17**, 67 (2005).
30. C. P. Brangwynne *et al.*, *J. Cell Biol.* **173**, 733 (2006).

Acknowledgments: We would like to thank J. Raff for providing the Dlic-GFP fly stock and centrosomal markers; H. Nash for providing the Mud antibody; S. Young for help with image analysis; and J. Guck, Y.-C. Oei, and P. K. Trong for help with the force calculations. This work was supported by a Wellcome Trust Principal Research Fellowship to D.St.J., Ph.D. scholarships from the FAZIT Stiftung, the Boehringer Ingelheim Fonds and the Cambridge European Trust to T.Z., the Gulbenkian Ph.D. scholarship of the Fundação para a Ciência e Tecnologia to A.R., and core support from the Wellcome Trust and Cancer Research UK.

Supplementary Materials

www.sciencemag.org/cgi/content/full/science.1219147/DC1
Materials and Methods
Figs. S1 to S8
References (*31*–*43*)
Movies S1 to S15

16 January 2012; accepted 27 March 2012
Published online 12 April 2012;
10.1126/science.1219147

Downloaded from www.sciencemag.org on May 29, 2012

Signatures of Majorana Fermions in Hybrid Superconductor-Semiconductor Nanowire Devices

V. Mourik,[1]* K. Zuo,[1]* S. M. Frolov,[1] S. R. Plissard,[2] E. P. A. M. Bakkers,[1,2] L. P. Kouwenhoven[1]†

Majorana fermions are particles identical to their own antiparticles. They have been theoretically predicted to exist in topological superconductors. Here, we report electrical measurements on indium antimonide nanowires contacted with one normal (gold) and one superconducting (niobium titanium nitride) electrode. Gate voltages vary electron density and define a tunnel barrier between normal and superconducting contacts. In the presence of magnetic fields on the order of 100 millitesla, we observe bound, midgap states at zero bias voltage. These bound states remain fixed to zero bias, even when magnetic fields and gate voltages are changed over considerable ranges. Our observations support the hypothesis of Majorana fermions in nanowires coupled to superconductors.

All elementary particles have an antiparticle of opposite charge (for example, an electron and a positron); the meeting of a particle with its antiparticle results in the annihilation of both. A special class of particles, called Majorana fermions, are predicted to exist that are identical to their own antiparticle (*1*). They may appear naturally as elementary particles or emerge as charge-neutral and zero-energy quasi-particles in a superconductor (*2*, *3*). Particularly interesting for the realization of qubits in quantum computing are pairs of localized Majoranas separated from each other by a superconducting region in a topological phase (*4*–*11*).

On the basis of earlier and later semiconductor-based proposals (*6*, *7*), Lutchyn *et al.* (*8*) and Oreg *et al.* (*9*) have outlined the necessary ingredients for engineering a nanowire device that should accommodate pairs of Majoranas. The starting point is a one-dimensional (1D) nanowire made of semiconducting material with strong spin-orbit interaction (Fig. 1A). In the presence of a magnetic field B along the axis of the nanowire (i.e., a Zeeman field), a gap is opened at the crossing between the two spin-orbit bands. If the Fermi energy μ is inside this gap, the degeneracy is twofold, whereas outside the gap it is fourfold. The next ingredient is to connect the semiconducting nanowire to an ordinary s-wave superconductor (Fig. 1A). The proximity of the superconductor induces pairing in the nanowire between electron states of opposite momentum and opposite spins and induces a gap, Δ. Combining this twofold degeneracy with an induced gap creates a topological superconductor (*4*–*11*). The condition for a topological phase is $E_Z > (\Delta^2 + \mu^2)^{1/2}$, with the Zeeman energy $E_Z = g\mu_B B/2$ (g is the Landé g factor, μ_B is the Bohr magneton). Near the ends of the wire, the electron density is reduced to zero, and subsequently, μ will drop below the subband energies such that μ^2 becomes large. At the points in space where $E_Z = (\Delta^2 + \mu^2)^{1/2}$, Majoranas arise as zero-energy (i.e., midgap) bound states—one at each end of the wire (*4*, *8*–*11*).

Despite their zero charge and energy, Majoranas can be detected in electrical measurements. Tunneling spectroscopy from a normal conductor into the end of the wire should reveal a state at zero energy (*12*–*14*). Here, we report the observation of such zero-energy peaks and show that they rigidly stick to zero energy while changing B and gate voltages over large ranges. Furthermore, we show that this zero-bias peak (ZBP) is absent if we take out any of the necessary ingredients of the Majorana proposals; that is, the rigid ZBP disappears for zero magnetic field, for a magnetic field parallel to the spin-orbit field, or when we take out the superconductivity.

[1]Kavli Institute of Nanoscience, Delft University of Technology, 2600 GA Delft, Netherlands. [2]Department of Applied Physics, Eindhoven University of Technology, 5600 MB Eindhoven, Netherlands.

*These authors contributed equally to this work.
†To whom correspondence should be addressed. E-mail: l.p.kouwenhoven@tudelft.nl

We use InSb nanowires (*15*), which are known to have strong spin-orbit interaction and a large *g* factor (*16*). From our earlier quantum-dot experiments, we extract a spin-orbit length $l_{so} \approx 200$ nm corresponding to a Rashba parameter $\alpha \approx 0.2$ eV·Å (*17*). This translates to a spin-orbit energy scale $\alpha^2 m^*/(2\hbar^2) \approx 50$ μeV ($m^* = 0.015 m_e$ is the effective electron mass in InSb, m_e is the bare electron mass, and $\hbar$ is Planck's constant h divided by 2π). Importantly, the *g* factor in bulk InSb is very large ($g \approx 50$), yielding $E_Z/B \approx 1.5$ meV/T. As shown below, we find an induced superconducting gap $\Delta \approx 250$ μeV. Thus, for $\mu = 0$, we expect to enter the topological phase for $B \sim 0.15$ T where E_Z starts to exceed Δ. The energy gap of the topological superconductor is estimated to be a few kelvin (*17*), if we assume a ballistic nanowire. The topological gap is substantially reduced in a disordered wire (*18*, *19*). We have measured mean free paths of ~300 nm in our wires (*15*), implying a quasi-ballistic regime in micrometer-long wires. With these numbers, we expect Majorana zero-energy states to become observable below 1 K and around 0.15 T.

A typical sample is shown in Fig. 1B. We first fabricate a pattern of narrow (50-nm) and wider (300-nm) gates on a silicon substrate (*20*). The gates are covered by a thin Si_3N_4 dielectric before we randomly deposit InSb nanowires. Next, we electrically contact those nanowires that have landed properly relative to the gates. The lower contact in Fig. 1B fully covers the bottom part of the nanowire. We have designed the upper contact to only cover half of the top part of the nanowire, avoiding complete screening of the underlying gates. This allows us to change the Fermi energy in the section of the nanowire (NW) with induced superconductivity. We have used either a normal (N) or superconducting (S) material for the lower and upper contacts, resulting in three sample variations: (i) N-NW-S, (ii) N-NW-N, and (iii) S-NW-S. Here, we discuss our main results on the N-NW-S devices, whereas the other two types, serving as control devices, are described in (*20*).

To perform spectroscopy on the induced superconductor, we created a tunnel barrier in the nanowire by applying a negative voltage to a narrow gate (dark green area in Fig. 1, B and C). A bias voltage applied externally between the N and S contacts drops almost completely across the tunnel barrier. In this setup, the differential conductance dI/dV at voltage V and current I is proportional to the density of states at energy $E = eV$ (where e is the charge on the electron) relative to the zero-energy dashed line in Fig. 1C. Figure 1D shows an example taken at $B = 0$. The two peaks at ±250 μeV correspond to the peaks in the quasi-particle density of states of the induced superconductor, providing a value for the induced gap, $\Delta \approx 250$ μeV. We generally find a finite dI/dV in between these gap edges. We observe pairs of resonances with energies symmetric around zero bias superimposed on nonresonant

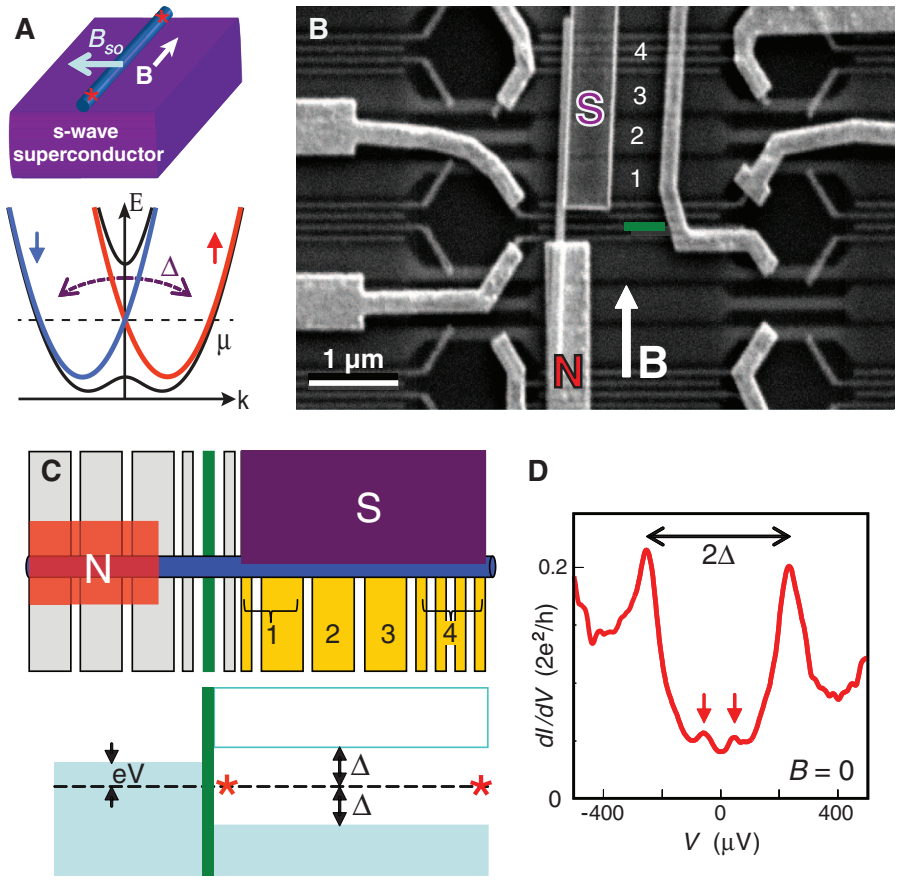

Fig. 1. (**A**) Outline of theoretical proposals. (Top) Conceptual device layout with a semiconducting nanowire in proximity to an s-wave superconductor. An external *B* field is aligned parallel to the wire. The Rashba spin-orbit interaction is indicated as an effective magnetic field, B_{so}, pointing perpendicular to the nanowire. The red stars indicate the expected locations of a Majorana pair. (Bottom) Energy, *E*, versus momentum, *k*, for a 1D wire with Rashba spin-orbit interaction, which shifts the spin-down band (blue) to the left and the spin-up band (red) to the right. Blue and red parabolas are for $B = 0$; black curves are for $B \neq 0$, illustrating the formation of a gap near $k = 0$ of size E_z (μ is the Fermi energy with $\mu = 0$ defined at the crossing of parabolas at $k = 0$). The superconductor induces pairing between states of opposite momentum and opposite spin, creating a gap of size Δ. (**B**) Implemented version of theoretical proposals. Scanning electron microscope image of the device with normal (N) and superconducting (S) contacts. The S contact only covers the right part of the nanowire. The underlying gates, numbered 1 to 4, are covered with a dielectric. [Note that gate 1 connects two gates, and gate 4 connects four narrow gates; see (C).] (**C**) (Top) Schematic of our device. (Bottom) illustration of energy states. The green rectangle indicates the tunnel barrier separating the normal part of the nanowire on the left from the wire section with induced superconducting gap, Δ. [In (B), the barrier gate is also shown in green.] An external voltage, *V*, applied between N and S drops across the tunnel barrier. Red stars again indicate the idealized locations of the Majorana pair. Only the left Majorana is probed in this experiment. (**D**) Example of differential conductance, dI/dV, versus *V* at $B = 0$ and 65 mK, serving as a spectroscopic measurement on the density of states in the nanowire region below the superconductor. Data are from device 1. The two large peaks, separated by 2Δ, correspond to the quasi-particle singularities above the induced gap. Two smaller subgap peaks, indicated by arrows, likely correspond to Andreev bound states located symmetrically around zero energy. Measurements are performed in dilution refrigerators with the use of the standard low-frequency lock-in technique (frequency = 77 Hz, excitation = 3 μV) in the four-terminal (devices 1 and 3) or two-terminal (device 2) current-voltage geometry.

currents throughout the gap region. Symmetric resonances likely originate from Andreev bound states (*21*, *22*), whereas nonresonant current indicates that the proximity gap has not fully developed (*23*).

Figure 2 summarizes our main result. Figure 2A shows a set of dI/dV-versus-V traces taken at increasing *B* fields in 10-mT steps from 0 (bottom trace) to 490 mT (top trace), offset for clarity. We again observe the gap edges at ±250 μeV. When we apply a *B* field between ~100 and ~400 mT along the nanowire axis, we observe a peak at $V = 0$. The peak has an amplitude up to ~$0.05 \cdot 2e^2/h$ and is clearly discernible from the background

Downloaded from www.sciencemag.org on May 29, 2012

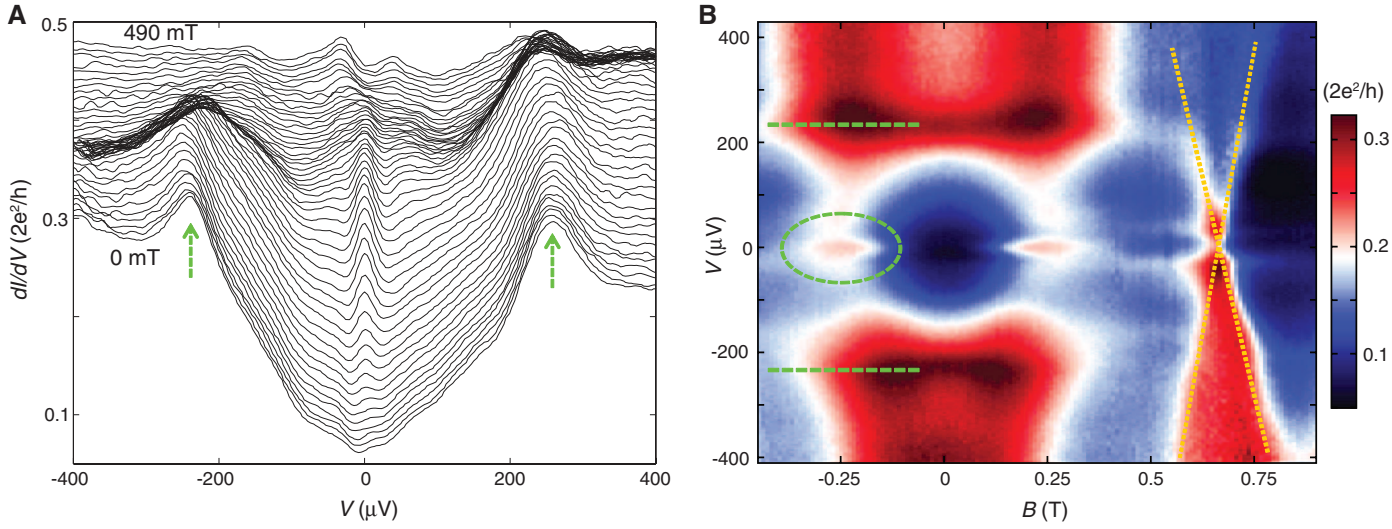

Fig. 2. Magnetic field–dependent spectroscopy. (**A**) *dI/dV* versus *V* at 70 mK taken at different *B* fields (from 0 to 490 mT in 10-mT steps; traces are offset for clarity, except for the lowest trace at $B = 0$). Data are from device 1. Arrows indicate the induced gap peaks. (**B**) Color-scale plot of *dI/dV* versus *V* and *B*. The ZBP is highlighted by a dashed oval; green dashed lines indicate the gap edges. At ~0.6 T, a non-Majorana state is crossing zero bias with a slope equal to ~3 meV/T (indicated by sloped yellow dotted lines). Traces in (A) are extracted from (B).

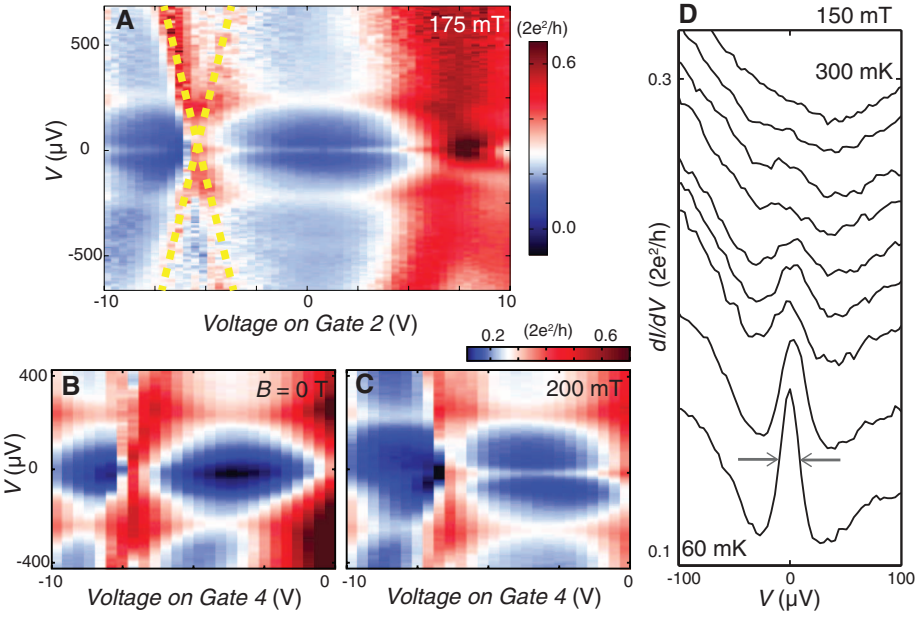

Fig. 3. Gate-voltage dependence. (**A**) A 2D color plot of *dI/dV* versus *V* and voltage on gate 2 at 175 mT and 60 mK. Andreev bound states cross through zero bias, for example, near −5 V (yellow dotted lines). The ZBP is visible from −10 to ~5 V (although in this color setting, it is not equally visible everywhere). Split peaks are observed in the range of 7.5 to 10 V (*20*). In (**B**) and (**C**), we compare voltage sweeps on gate 4 for 0 and 200 mT with the ZBP absent and present, respectively. Temperature is 50 mK. [Note that in (C) the peak extends all the way to −10 V (*19*).] (**D**) Temperature dependence. *dI/dV* versus *V* at 150 mT. Traces have an offset for clarity (except for the lowest trace) and are taken at different temperatures (from bottom to top: 60, 100, 125, 150, 175, 200, 225, 250, and 300 mK). *dI/dV* outside the ZBP at $V = 100$ μeV is $0.12 \pm 0.01 \cdot 2e^2/h$ for all temperatures. A FWHM of 20 μeV is measured between the arrows. All data in this figure are from device 1.

conductance. Above ~400 mT, we observe a pair of peaks. The color panel in Fig. 2B provides an overview of states and gaps in the plane of energy and *B* field from −0.5 to 1 T. The observed symmetry around $B = 0$ is typical for all of our data sets, demonstrating reproducibility and the absence of hysteresis. We indicate the gap edges with horizontal green dashed lines (highlighted only for $B < 0$). A pair of resonances crosses zero energy at ~0.65 T with a slope on the order of E_Z (highlighted by orange dotted lines). We have followed these resonances up to high bias voltages in (*20*) and identified them as Andreev states bound within the gap of the bulk NbTiN superconducting electrodes (~2 meV). In contrast, the ZBP sticks to zero energy over a range of $\Delta B \sim 300$ mT centered around ~250 mT. Again at ~400 mT, we observe two peaks located at symmetric, finite biases.

To identify the origin of these ZBPs, we need to consider various options including the Kondo effect, Andreev bound states, weak antilocalization, and reflectionless tunneling versus a conjecture of Majorana bound states. ZBPs due to the Kondo effect (*24*) or Andreev states bound to s-wave superconductors (*25*) can occur at finite *B*; however, with changing *B*, these peaks then split and move to finite energy. A Kondo resonance moves with $2E_Z$ (*24*), which is easy to dismiss as the origin for our ZBP because of the large *g* factor in InSb. (Note that even a Kondo effect from an impurity with $g = 2$ would be discernible.) Reflectionless tunneling is an enhancement of Andreev reflection by time-reversed paths in a diffusive normal region (*26*). As in the case of weak antilocalization, the resulting ZBP is maximal at $B = 0$ and disappears when *B* is increased; see also (*20*). We thus conclude that the above options for a ZBP do not provide natural explanations for our observations. We are not aware of any mechanism that could explain our observations, besides the conjecture of a Majorana.

To further investigate the zero-biasness of our peak, we measured gate voltage dependences. Figure 3A shows a color panel with voltage sweeps on gate 2. The main observation is the occurrence of two opposite types of behavior. First, we observe peaks in the density of

Downloaded from www.sciencemag.org on May 29, 2012

states that change with energy when changing gate voltage (highlighted with yellow dotted lines); these are the same resonances as shown in Fig. 2B and analyzed in (*20*). The second observation is that the ZBP from Fig. 2, which we take at 175 mT, remains stuck to zero bias while changing the gate voltage over a range of several volts. Clearly, our gates work because they change the Andreev bound states by ~0.2 meV per volt on the gate. Panels (B) and (C) in Fig. 3 underscore this observation with voltage sweeps on a different gate, number 4. Fig. 3B shows that, at zero magnetic field, no ZBP is observed. At 200 mT, the ZBP becomes again visible in Fig. 3C. Comparing the effect of gates 2 and 4, we observe that neither moves the ZBP away from zero.

Initially, Majorana fermions were predicted in single-subband, 1D wires (*8*, *9*), but further work extended these predictions to multisubband wires (*27*–*30*). In the nanowire section that is uncovered, we can gate tune the number of occupied subbands from 0 to ~4 with subband separations of several millielectron volts. Gate tuning in the nanowire section covered with superconductor is much less effective due to efficient screening. The number of occupied subbands in this part is unknown, but it is most likely multiple subbands. As shown in figs. S9 and S11 of (*20*), we do have to tune gate 1 and the tunnel barrier to the right regime to observe the ZBP.

We have measured in total several hundred panels sweeping various gates on different devices. Our main observations are (i) a ZBP exists over a substantial voltage range for every gate starting from the barrier gate until gate 4, (ii) we can occasionally split the ZBP in two peaks located symmetrically around zero, and (iii) we can never move the peak away from zero to finite bias (*20*). Data sets such as those in Figs. 2 and 3 demonstrate that the ZBP remains stuck to zero energy over considerable changes in B and gate voltage V_g.

Figure 3D shows the temperature dependence of the ZBP. We find that the peak disappears at ~300 mK, providing a thermal-energy scale of $k_BT \sim 30$ μeV (where k_B is Boltzmann constant and T is temperature). The full width at half maximum (FWHM) at the lowest temperature is ~20 μeV, which we believe is a consequence of thermal broadening as $3.5 \cdot k_BT(60\ \text{mK}) = 18$ μeV.

Next, we verify explicitly that all the required ingredients in the theoretical Majorana proposals (Fig. 1A) are indeed essential for observing the ZBP. We have already verified that a nonzero B field is needed. We then test to see whether spin-orbit interaction is crucial for the absence or presence of the ZBP. Theory requires that the external B has a component perpendicular to B_{so} (the spin-orbit magnetic field). We have measured a second device in a different setup containing a 3D vector magnet such that we can sweep the B field in arbitrary directions. In Fig. 4, we show dI/dV versus V while varying the angle for a constant field magnitude. In Fig. 4A, the plane of rotation is approximately equal to the plane of the substrate. We clearly observe that the ZBP comes and goes, depending on the angle. The ZBP is completely absent around π/2, which we thus deduce as the direction of B_{so}. In Fig. 4B, the plane of rotation is perpendicular to B_{so}. Indeed, we observe that the ZBP is now present for all angles, because B is now always perpendicular to B_{so}. These observations are in full agreement with expectations for the spin-orbit direction in our samples (*17*, *31*). We have further verified that this angle dependence is not a result of the specific magnitude of B or a variation in g factor (*20*).

As a last check, we have fabricated and measured a device of identical design but with the superconductor replaced by a normal Au contact (that is, a N-NW-N geometry). In this sample, we have not found any signature of a peak that sticks to zero bias while changing both B and V_g (*20*). This test experiment shows that superconductivity is also an essential ingredient for our ZBP.

To summarize, we have reproduced our observation of a rigid ZBP in three different devices and in two different setups. Our general observations are: (i) a ZBP appears at finite B and sticks to zero bias over a range from 0.07 to 1 T; (ii) the ZBP remains at zero bias while changing the voltage on any of our gates over large ranges; (iii) the ZBP comes and goes with the angle of the B field with respect to the wire axis, which is in agreement with the expected spin-orbit interaction; and (iv) the rigid ZBP is

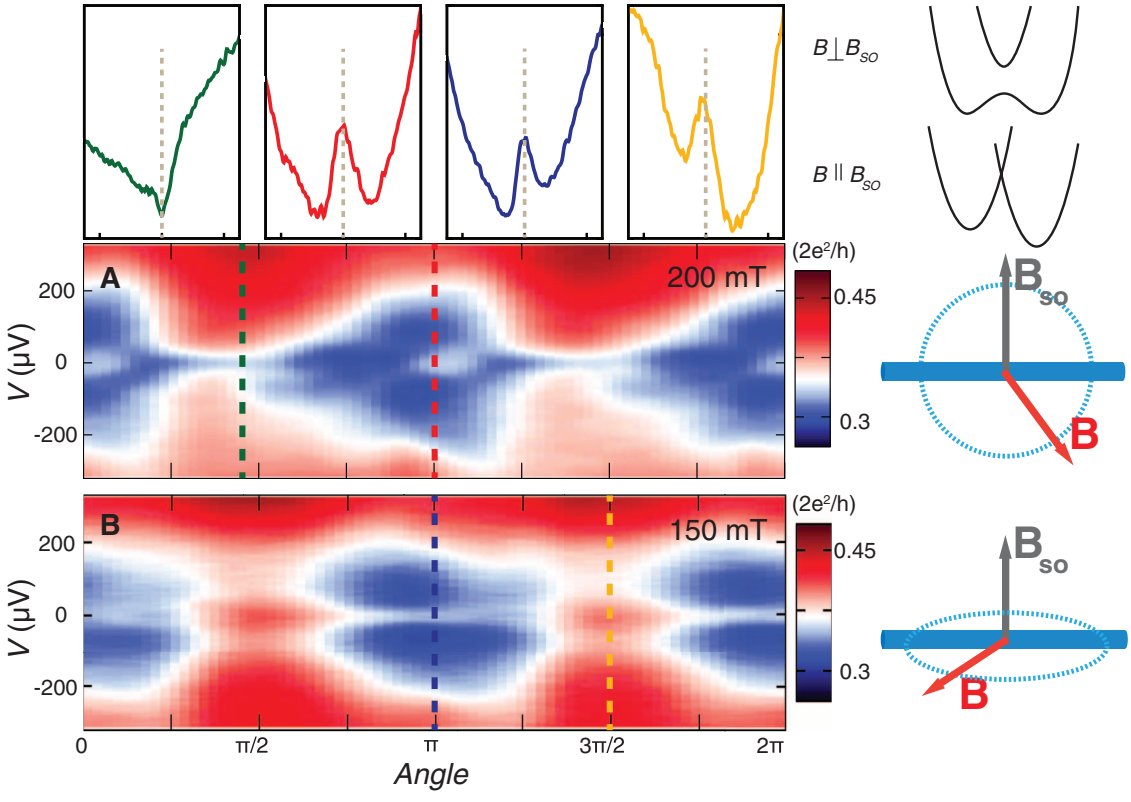

Fig. 4. Magnetic-field orientation dependence. *dI*/*dV* versus *V* and varying the angle of *B* at fixed magnitude. Data from device 2 are measured in a different setup at ~150 mK; zero angle is along the nanowire for both panels. (**A**) Rotation of $|B| = 200$ mT in the plane of the substrate. The ZBP is at a maximum when *B* is parallel and is absent when *B* is perpendicular to the wire. (**B**) Rotation of $|B| = 150$ mT in the plane perpendicular to B_{so}. The ZBP is now present for all angles. The panels on top show linecuts at angles with corresponding colors in (A) and (B). Panels on the right side illustrate, from top to bottom: (i) For *B* perpendicular to B_{so} a gap opens lifting fermion doubling, as is required for Majoranas. (ii) For *B* parallel to B_{so}, the two spin bands from Fig. 1A shift vertically by $2E_Z$. In this configuration, a zero-energy Majorana is not expected. (iii) Panel of rotation of *B* for data in (A) is shown. (iv) Panel of rotation of *B* for data in (B) is shown.

Downloaded from www.sciencemag.org on May 29, 2012

absent when the superconductor is replaced by a normal conductor. Based on these observations, we conclude that our spectroscopy experiment provides evidence for the existence of Majorana fermions.

Improving the electron mobility and optimizing the gate coupling will enable us to map out the phase diagram of the topological superconductor in the plane of E_Z and μ (*27*–*30*). It will be interesting to control the subband occupation underneath the superconductor down to a single subband to make direct comparisons to theoretical models. Currently, we probe induced gaps and states from all occupied subbands, each with a different coupling to the tunnel barrier. The topological state in the topmost subband likely has the weakest coupling to the tunnel barrier. Single-subband models (*8*, *9*) predict that one should observe a closing of the topological gap; however, in multisubband systems, this gap closing may not be visible. The constant gap in Fig. 2 may come from lower subbands. The presence of multiple subbands together with our finite temperature may also be the reason that our ZBP is currently only ~5% of the theoretical zero-temperature limit of $2e^2/h$ (*12*, *14*).

Finally, we note that this work does not address the topological properties of Majorana fermions. The first step toward demonstrating topological protection would be the observation of conductance quantization (*12*, *32*). Second, in a Josephson tunnel junction with phase difference φ and a pair of Majoranas on either side, the current-phase relation becomes proportional to sin(φ/2). The factor 2 is another distinct Majorana signature, which should be observable as an *h*/*e* flux periodicity in a superconducting quantum interference device measurement (*8*, *9*). The last type of experiment involves the exchange of Majoranas around each other. Such braiding experiments can reveal their non-Abelian statistics, which are the ultimate proof of topologically protected Majorana fermions (*33*–*35*).

References and Notes

1. E. Majorana, *Soryushiron Kenkyu* (Engl. transl.) **63**, 149 (1981) [translation from *Nuovo Cimento* **14**, 171 (1937)].
2. F. Wilczek, *Nat. Phys.* **5**, 614 (2009).
3. M. Franz, *Physics* **3**, 24 (2010).
4. A. Yu. Kitaev, *Phys. Usp.* **44**, 131 (2001).
5. L. Fu, C. L. Kane, *Phys. Rev. Lett.* **100**, 096407 (2008).
6. J. D. Sau, R. M. Lutchyn, S. Tewari, S. Das Sarma, *Phys. Rev. Lett.* **104**, 040502 (2010).
7. J. Alicea, *Phys. Rev. B* **81**, 125318 (2010).
8. R. M. Lutchyn, J. D. Sau, S. Das Sarma, *Phys. Rev. Lett.* **105**, 077001 (2010).
9. Y. Oreg, G. Refael, F. von Oppen, *Phys. Rev. Lett.* **105**, 177002 (2010).
10. C. W. J. Beenakker, http://arxiv.org/abs/1112.1950 (2011).
11. J. Alicea, http://arxiv.org/abs/1202.1293 (2012).
12. K. T. Law, P. A. Lee, T. K. Ng, *Phys. Rev. Lett.* **103**, 237001 (2009).
13. K. Flensberg, *Phys. Rev. B* **82**, 180516 (2010).
14. J. D. Sau, S. Tewari, R. Lutchyn, T. Stanescu, S. Das Sarma, *Phys. Rev. B* **82**, 214509 (2010).
15. S. R. Plissard *et al.*, *Nano Lett.* **12**, 1794 (2012).
16. H. A. Nilsson *et al.*, *Nano Lett.* **9**, 3151 (2009).
17. S. Nadj-Perge *et al.*, *Phys. Rev. Lett.* **108**, 166801 (2012).
18. P. W. Brouwer, M. Duckheim, A. Romito, F. von Oppen, *Phys. Rev. Lett.* **107**, 196804 (2011).
19. J. D. Sau, S. Tewari, S. Das Sarma, *Phys. Rev. B* **85**, 064512 (2012).
20. See supplementary materials on *Science* Online.
21. J. D. Pillet *et al.*, *Nat. Phys.* **6**, 965 (2010).
22. T. Dirks *et al.*, *Nat. Phys.* **7**, 386 (2011).
23. H. le Sueur, P. Joyez, H. Pothier, C. Urbina, D. Esteve, *Phys. Rev. Lett.* **100**, 197002 (2008).
24. S. Sasaki *et al.*, *Nature* **405**, 764 (2000).
25. M. Zareyan, W. Belzig, Yu. V. Nazarov, *Phys. Rev. B* **65**, 184505 (2002).
26. B. J. van Wees, P. de Vries, P. Magnée, T. M. Klapwijk, *Phys. Rev. Lett.* **69**, 510 (1992).
27. M. Wimmer, A. R. Akhmerov, M. V. Medvedyeva, J. Tworzydło, C. W. Beenakker, *Phys. Rev. Lett.* **105**, 046803 (2010).
28. A. C. Potter, P. A. Lee, *Phys. Rev. Lett.* **105**, 227003 (2010).
29. R. M. Lutchyn, T. D. Stanescu, S. Das Sarma, *Phys. Rev. Lett.* **106**, 127001 (2011).
30. T. D. Stanescu, R. M. Lutchyn, S. Das Sarma, *Phys. Rev. B* **84**, 144522 (2011).
31. P. Středa, P. Šeba, *Phys. Rev. Lett.* **90**, 256601 (2003).
32. M. Wimmer, A. R. Akhmerov, J. P. Dahlhaus, C. W. J. Beenakker, *N. J. Phys.* **13**, 053016 (2011).
33. N. Read, D. Green, *Phys. Rev. B* **61**, 10267 (2000).
34. D. A. Ivanov, *Phys. Rev. Lett.* **86**, 268 (2001).
35. C. Nayak, S. H. Simon, A. Stern, M. Freedman, S. Das Sarma, *Rev. Mod. Phys.* **80**, 1083 (2008).

Acknowledgments: We thank D. Thoen and T. Klapwijk for sharing their NbTiN technology and A. Akhmerov, J. Alicea, C. Beenakker, M. Freedman, F. Hassler, G. Immink, H. Keijzers, C. Marcus, S. Nadj-Perge, Y. Nazarov, I. van Weperen, M. Wimmer, and D. van Woerkom for discussions and assistance. This work has been supported by European Research Council, Netherlands Organization for Scientific Research (NWO), Foundation for Fundamental Research on Matter (FOM), and Microsoft Corporation Station Q.

Supplementary Materials

www.sciencemag.org/cgi/content/full/science.1222360/DC1
Supplementary Text
Figs. S1 to S14
References (*36*, *37*)
Data Files

23 March 2012; accepted 5 April 2012
Published online 12 April 2012;
10.1126/science.1222360

Downloaded from www.sciencemag.org on May 29, 2012

Unidirectional Growth of Microbumps on (111)-Oriented and Nanotwinned Copper

Hsiang-Yao Hsiao,[1] Chien-Min Liu,[1] Han-wen Lin,[1] Tao-Chi Liu,[1] Chia-Ling Lu,[1] Yi-Sa Huang,[1] Chih Chen,[1]* K. N. Tu[2]*

Highly oriented [111] Cu grains with densely packed nanotwins have been fabricated by direct-current electroplating with a high stirring rate. The [111]-oriented and nanotwinned Cu (nt-Cu) allow for the unidirectional growth of Cu_6Sn_5 intermetallics in the microbumps of three-dimensional integrated-circuit packaging; a uniform microstructure in a large number of microbumps of controlled orientation can be obtained. The high-density twin boundaries in the nt-Cu serve as vacancy sinks during the solid-state reaction between Pb-free solder and Cu and greatly reduce the formation of Kirkendall (or Frenkel) voids.

A change from two-dimensional to three-dimensional integrated circuits (3D IC) is under way in the microelectronics industry as the limits of very-large-scale integration in silicon chip technology are approached (*1*). In essence, 3D IC is intended to bring packaging technology and chip technology together. With respect to scaling the density of solder bumps on a chip surface, the diameter of a flip-chip solder bump is about 100 μm today, and it should be possible to reduce this to 1 μm. This improvement will increase the density of bumps per unit area by 4 orders of magnitude, yet the solder volume will be reduced by 6 orders of magnitude. However, the melting point of the solder remains unchanged, meaning that each microbump may contain only a few grains after processing. Variation in the grain orientation may lead to a wide distribution of the orientation-dependent properties of microbumps, which may in turn lead to early failure and low reliability. This is because certain grain orientations allow fast diffusion and electromigration (*2*, *3*). Because there are a large number of microbumps on a stack of chips in a 3D IC, achieving a uniform microstructure in several thousand of these microbumps on each chip is a critical issue.

Maintaining control over the microstructure of the microbumps is nontrivial because of

[1]Department of Materials Science and Engineering, National Chiao Tung University, Hsinchu, Taiwan 30010, Republic of China. [2]Department of Materials Science and Engineering, University of California at Los Angeles, Los Angeles, CA 90095, USA.

*To whom correspondence should be addressed. E-mail: chih@mail.nctu.edu.tw (C.C.); kntu@ucla.edu (K.N.T.)